

The Exact Potential Driving the Electron Dynamics in Enhanced Ionization

Elham Khosravi,^{1,2,*} Ali Abedi,^{1,2,†} and Neepa T. Maitra^{1,‡}

¹Department of Physics and Astronomy, Hunter College and the Graduate Center of the City University of New York, 695 Park Avenue, New York, New York 10065, USA

²Nano-Bio Spectroscopy Group and European Theoretical Spectroscopy Facility (ETSF), Universidad del País Vasco CFM CSIC-UPV/EHU-MPC and DIPC, Av. Tolosa 72, 20018 San Sebastián, Spain

(Dated: November 7, 2021)

It was recently shown that the exact factorization of the electron-nuclear wavefunction allows the construction of a Schrödinger equation for the electronic system, in which the potential contains exactly the effect of coupling to the nuclear degrees of freedom and any external fields. Here we study the exact potential acting on the electron in charge-resonance enhanced ionization in a model one-dimensional H_2^+ molecule. We show there can be significant differences between the exact potential and that used in the traditional quasistatic analyses, arising from non-adiabatic coupling to the nuclear system, and that these are crucial to include for accurate simulations of time-resolved ionization dynamics and predictions of the ionization yield.

Ionization is a fundamental process in the strong-field physics of atoms and molecules, lying at the heart of many fascinating phenomena such as high harmonic generation, Coulomb explosion, laser induced electron diffraction, and molecular orbital tomography. The ionization rate from a molecule can be several orders of magnitude higher than the rate from the constituent atoms at a critical range of internuclear separations. This phenomenon, termed charge-resonance enhanced ionization (CREI), was first theoretically predicted about twenty years ago [1–4], and soon after verified experimentally [5–7].

The enhancement in the ionization rate has been explained by a quasistatic argument in the pioneering works of Ref [2, 4, 8–11], treating the nuclei as instantaneously-fixed point particles, with the electrons following the combined potential from the laser field and the electrostatic attraction of the nuclei. In any experiment however, the nuclei are neither frozen, nor are they point particles; instead their motion can be *strongly* coupled to the electron dynamics and accounting for the coupled electron-ion quantum dynamics can be essential [12]. Further, the electron does not simply follow the field adiabatically, evidenced by the multiple subcycle ionization bursts recently revealed in Refs. [13, 14]. A handful of calculations treating the full dynamics of quantum nuclei and the electron in H_2^+ [4, 8], as well as a few experiments, have verified that the essential CREI phenomenon remains robust, although the details are altered by the ionic dynamics. For example, in Refs. [5] it was found that nuclear motion washes out the two-peak structure predicted in the frozen-nuclei analysis of CREI [2] into a single broad peak. Further, the CREI enhancement is subdued if, during the experiment, only little of the nuclear density reaches the critical internuclear separation [15]. Hence, to properly understand, model, and predict the experiment, a fully time-dependent picture of coupled electronic and ionic motion is needed.

In this Letter, we utilize the exact factorization approach [16–19] to investigate the dynamics of the electron during the CREI process, as influenced by the field and nuclear wavepacket dynamics. In particular, we study the exact time-dependent potential that drives the electron and fully accounts for coupling to both the field and the dynamical nuclei. This concept has been introduced by the exact factorization in its inverse form [18], and here we show that, for the CREI process, this exact potential can be remarkably different from the quasistatic potential, or even from a modified quasistatic potential that accounts for the width and splitting of the nuclear wavepacket. This indicates the need for dynamical electron-nuclear correlation effects to be included in the calculation. Further, we identify a new measure of ionization appropriate for fully dynamical studies, which indicates the regions of the nuclear wavepacket associated with the ionizing electron.

By restricting the motion of the nuclei and the electron in the H_2^+ molecule to the polarization direction of the laser field the problem can be modeled with a one-dimensional Hamiltonian featuring “soft-Coulomb” interactions [20] (atomic units, $e = m = \hbar = 1$, are used throughout the article, unless otherwise noted):

$$\hat{H}(t) = -\frac{1}{2\mu_e} \frac{\partial^2}{\partial z^2} - \frac{1}{M} \frac{\partial^2}{\partial R^2} - \frac{1}{\sqrt{1 + (z - R/2)^2}} - \frac{1}{\sqrt{1 + (z + R/2)^2}} + \frac{1}{\sqrt{0.03 + R^2}} + \hat{V}_I(z, t) \quad (1)$$

where R and z are the internuclear distance and the electronic coordinate as measured from the nuclear center-of-mass, respectively. The proton mass is denoted as M while $\mu_e = (2M)/(2M + 1)$ is the electronic reduced mass. The laser field, within the dipole approximation, is represented by $\hat{V}_I(z, t) = q_e z E(t)$ where $E(t)$ denotes the electric field amplitude and the reduced charge $q_e = (2M + 2)/(2M + 1)$. Such reduced-dimensional models have been shown to qualitatively reproduce experimen-

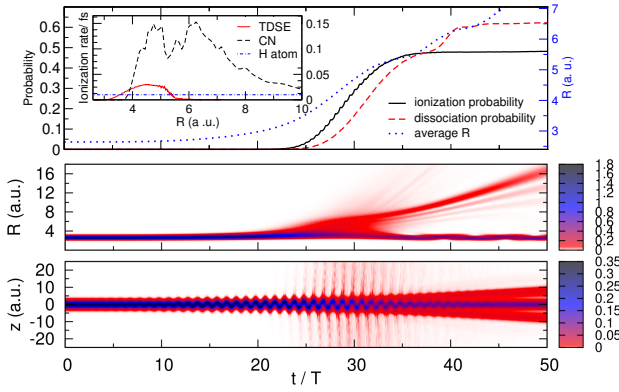


FIG. 1. Upper panel: Ionization probability, dissociation probability, average internuclear distance $\langle R \rangle$, as a function of number of cycles t/T . The inset depicts the ionization rate for: clamped-nucleus (CN) calculation, as a function of the internuclear distance (black dashed curve), the exact molecular TDSE as a function of $\langle R \rangle$ (red full curve), and the H atom (dash dotted line). Middle panel: contour plot of the time-dependent nuclear density. Lower panel: contour plot of time-dependent electronic density.

tal results (see Ref. [21] for example). Here we first study the dynamics of the system subject to a 50-cycle pulse of wavelength $\lambda = 800$ nm ($\omega = 0.0569$ a.u.) and intensity $I = 2 \times 10^{14}$ W/cm², with a sine-squared pulse envelope.

Setting the ground-state of the molecule as the initial state, we first solve the time-dependent Schrödinger equation (TDSE) for Hamiltonian in Eq. (1) numerically exactly. The upper panel of Figure 1, shows the ionization probability, dissociation probability and the average internuclear distance $\langle R \rangle$ as a function of number of optical cycles (t/T) [22]. Here T denotes duration of one cycle which in this case is $T = 2.67$ fs. We see from the figure that ionization is rapidly onset as we approach the middle of the pulse, slowing down later while the field decreases. The nuclei dissociate primarily via Coulomb explosion following ionization. Note that the majority of the ionization occurs when $\langle R \rangle$ is between 4–5.5 a.u. The inset of the upper panel of Figure (1) shows the ionization rate which in the fully dynamical calculation, is plotted against the average internuclear separation $\langle R \rangle(t)$, while in the clamped-nuclei (CN) case, it is calculated and plotted for each fixed internuclear separation R [23]. In the CN case, the peak near 6.5 a.u. is usually identified with CREI while that near 5 a.u. is associated with a symmetry-breaking electron localization [2]. The exact ionization rate, however, has a single broad peak centered between 4 a.u. and 5 a.u., and is smaller than that of the CN calculations, but still higher than the atomic rate, similar to the observations in Refs. [4, 5].

One should keep in mind that representing the ionization rate in the fully-dynamical case as a function of just

the average internuclear separation has however only limited meaning: the nuclear charge distribution, plotted in the middle panel of Figure 1, bifurcates, so considering ionization simply as a function of the average separation does not properly indicate the internuclear separations at which the ionization rate is enhanced. A large fragment of the nuclear density remains localized, oscillating around the equilibrium separation, while another part begins to dissociate, soon after the ionization is onset. This can be seen clearly in the plot of the electronic density plotted in the lower panel of Figure 1. Hence a dynamical picture of the CREI that accounts for the coupling to the nuclear distribution as it changes in time is desirable.

A complete picture of the electronic dynamics coupled to the non-classical nuclei is provided within the exact factorization framework in its *inverse* formulation [18]: Complementary to the direct factorization of Refs. [16, 17], the exact electron-nuclear wavefunction $\Psi(\underline{\mathbf{r}}, \underline{\mathbf{R}}, t)$ that solves the full electron-nuclear TDSE can be exactly written as a product $\Psi(\underline{\mathbf{r}}, \underline{\mathbf{R}}, t) = \Phi(\underline{\mathbf{r}}, t) \chi_{\underline{\mathbf{r}}}(\underline{\mathbf{R}}, t)$, where $\Phi(\underline{\mathbf{r}}, t)$ may be interpreted as the electronic wavefunction and $\chi_{\underline{\mathbf{r}}}(\underline{\mathbf{R}}, t)$ the conditional nuclear wavefunction that parametrically depends on the electronic configuration $\underline{\mathbf{r}}$ and satisfies the partial normalization condition $\int d\underline{\mathbf{R}} |\chi_{\underline{\mathbf{r}}}(\underline{\mathbf{R}}, t)|^2 = 1$ for every $\underline{\mathbf{r}}$ at each t . The electronic wavefunction can be shown to yield the exact N_e -body electronic density, and N_e -body electronic current-density of the system. The equations of motion that the electronic and nuclear factors satisfy are presented in [18]. The electronic equation, in particular, has the appealing form of a TDSE that contains an exact time-dependent scalar potential as well as a time-dependent vector potential: for any one-dimensional case, we can choose a gauge such that the vector potential is zero [16–18], and then:

$$\left(-\frac{1}{2\mu} \frac{\partial^2}{\partial z^2} + \epsilon_e(z, t) \right) \Phi(z, t) = i \partial_t \Phi(z, t). \quad (2)$$

Hence, the exact potential driving the electron dynamics is $\epsilon_e(z, t)$ which can be compared with the traditional potentials used to study electronic dynamics. This potential, termed the time-dependent potential energy surface for electrons, *e*-TDPES, can be decomposed to

$$\epsilon_e(z, t) = \epsilon^{\text{app}}(z, t) + \mathcal{T}_n(z, t) + \mathcal{K}_e^{\text{cond}}(z, t) + \epsilon_e^{\text{gd}}(z, t), \quad (3)$$

where for our H_2^+ model,

$$\begin{aligned} \epsilon^{\text{app}}(z, t) = & \langle \chi_z(R, t) | \hat{W}_{en}(z, R) + \hat{W}_{nn}(R) | \chi_z(R, t) \rangle_R \\ & + \hat{V}^l(z, t), \end{aligned} \quad (4)$$

is an approximate potential that generalizes the traditional quasistatic potential to the case of a quantum nuclear wavepacket. The second term,

$$\mathcal{T}_n(z, t) = - \langle \chi_z(R, t) | \partial_R^2 | \chi_z(R, t) \rangle_R / M, \quad (5)$$

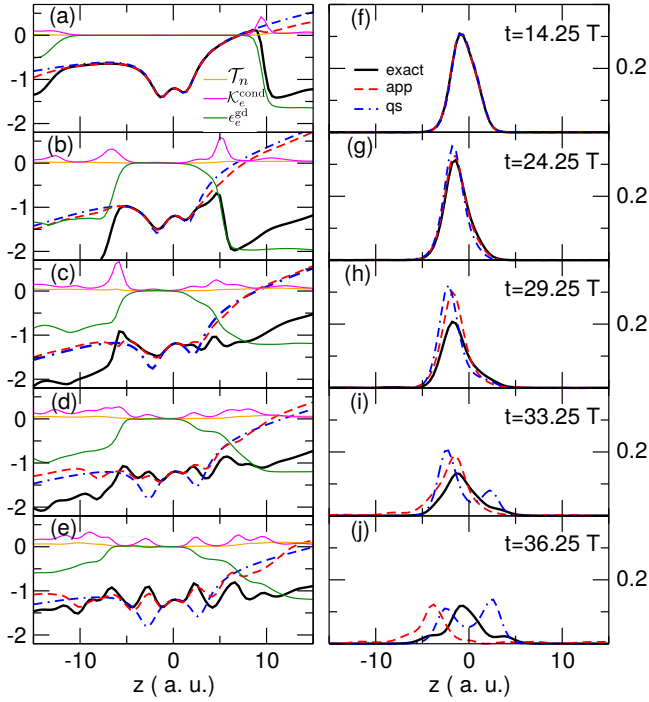


FIG. 2. The exact electronic potential ϵ_e (black solid line) and its various components together with the quasistatic potential ϵ^{qs} (blue dash line) are plotted in the left-hand side at five different snapshots of time. The exact electron density together with the electron density calculated from propagating the electron on ϵ^{qs} and ϵ^{app} are plotted on the right-hand side.

represents a nuclear-kinetic contribution to the electronic potential from the conditional nuclear wavefunction, while,

$$\mathcal{K}_e^{\text{cond}}(z, t) = \langle \partial_z \chi_z(R, t) | \partial_z \chi_z(R, t) \rangle_R / M, \quad (6)$$

represents an electronic-kinetic-like contribution from the conditional nuclear wavefunction, and,

$$\epsilon_e^{\text{gd}}(z, t) = \langle \chi_z(R, t) | -i \partial_t | \chi_z(R, t) \rangle_R, \quad (7)$$

is the gauge-dependent component of the potential. It is important to note that ϵ^{app} reduces to the quasistatic potential when the nuclear density is approximated classically as a z -independent delta-function at $\bar{R}(t) = \langle R \rangle(t)$:

$$\epsilon^{\text{qs}}(z, t | \bar{R}(t)) = \hat{W}_{en}(z, \bar{R}(t)) + \hat{W}_{nn}(\bar{R}(t)) + \hat{V}^l(z, t). \quad (8)$$

We now investigate the e -TDPES (Eq. 3) and discuss the impact of its components (Eqs. 4–7) on the electron dynamics. In particular, we ask how well electron propagation on ϵ^{app} performs: is accounting for the width of the nuclear wavepacket, and its correlation with the electron dynamics via the parametric dependence, enough to capture accurately the full electron dynamics? In Figure 2 the exact e -TDPES, ϵ_e , (black solid line) and its various components together with the

quasistatic potential ϵ^{qs} (blue dash line) are plotted on the left-hand side at five different snapshots of time in which the field is at the maximum of the cycle. The exact electron density together with the electron density calculated from propagating the electron on ϵ^{qs} and ϵ^{app} are plotted on the right-hand side. In all these calculations, the initial state is chosen to be the exact ground state density of the complete system. We also plot the ionization yields calculated from propagating the electron on different components of the exact electronic potential on the left on Fig. 3.

We have chosen times that are representative of three different phases of the dynamics (refer to Fig. 1): (1) the initial phase, up to $t \approx 20T$, for which the dissociation and ionization probabilities are still negligible (panel (a) of Fig. 2, shown at $t = 14.25T$), (2) the second phase, $\sim 20T < t < \sim 35T$, which is when ionization/dissociation mostly occurs; panels (b)–(d) of Fig. 2 ($t = 24.25, 29.25, 33.25T$) are chosen to illustrate this phase, (3) the final phase, $t > 35T$, in which the system begins to stabilize, while the field intensity decreases, represented at $t = 36.25T$ in panel (e).

In the first phase of the dynamics (representative panel (a)), the nuclear wavepacket is quite localized around its initial position and the e -TDPES, quasistatic potential and approximate potential are essentially on top of each other in the central region ($|z| < 10$ a.u.). They differ from each other only in the tail of the electronic density, where, in particular, ϵ_e has a large step downward (Fig. 2(a)). Since the density is very tiny in the tail region, the overall dynamics is not affected significantly by this feature. In the second phase of the dynamics the nuclear motion begins to pick up, affecting the shape of the exact e -TDPES in the central region. From this point on the exact potential begins to develop features that are absent in the quasistatic potential. As part of the nuclear density begins to stretch apart, the e -TDPES begins to exhibit a double well structure in the up-field side of the potential ($0 < z < 5$ a.u.), while the down-field side maintains a single well structure as is shown in panels (b) and (c). Further, the depth of the central wells are decreased compared to the quasistatic picture. Outside the central region ($|z| > 5$ a.u.) the e -TDPES drops down, yielding a barrier that is smaller and narrower than that of the quasistatic potential. This feature in particular, significantly facilitates the tunnelling ionization of the electron density in the exact dynamics already at $t = 24.25T$, evident in the spreading of the exact density (panel (g), see also left panel of Fig. 3). In the case of the quasistatic and approximate potentials, the ionization is still negligible at this time, due to small tunnelling probability. The differences between the exact e -TDPES and both ϵ^{app} and ϵ^{qs} continue to grow in the central region ($|z| < 5$ a.u.) throughout the second phase (panels (b)–(d), and corresponding electronic densities (g)–(i)), as contributions from ϵ_e^{gd}

and $\mathcal{K}_e^{\text{cond}}$ get larger and extend closer to the center. It is interesting to note that ϵ_e^{gd} typically has large steps that lowers the potential on both sides, allowing for more ionization (see also Fig. 3, left panel), while $\mathcal{K}_e^{\text{cond}}$ develops several (smaller) barrier structures, whose net effect also appears to increase the ionization yield in this phase (see Fig. 3). The \mathcal{T}_n term has very small barriers in the outer region whose tendency is to confine the density, leading to a decrease in the ionization probability.

By the end of the second phase, at $t = 33.25 T$ (Fig. 2 (d)), the exact potential is totally different from the quasistatic potential, everywhere except for at small $|z| < 1$, presenting a shallow double well structure in both up-field and down-field sides of the potential. Furthermore, the discrepancy between the ϵ^{qs} and ϵ^{app} becomes more noticeable as the nuclear wavepacket begins to split and dissociate in the field. By this time, there has been significant ionization in all three cases (left panel of Fig. 3), although more in the exact case, as discussed above. Towards the end of the second phase, the ionization yields of the quasistatic and approximate calculations begin to differ from each other, as expected from the growing discrepancy between their respective potentials.

Entering now the third phase of the dynamics, four optical cycles later (panel (e) in Fig. 2), the exact potential differs dramatically from the other two showing a formation of four wells in the central region ($|z| < 6$ a.u.). The two wells in the center are associated with the part of the nuclear density that is not dissociated while the other two are associated with the dissociating fragment, and hence, they move outwards. The e -TDPES consequently localizes the electronic density in three positions as seen in panel (j) of Fig. 2, namely in the center corresponding to the part of the nuclear density that is localized around the equilibrium, and on each of the dissociating fragments of protons. In the third phase, ϵ^{app} grossly overionizes the system; as ϵ^{app} has many shallow barriers and continues to oscillate in the field, failing to stabilize. The quasistatic potential ϵ^{qs} retains a deep double well structure throughout the dynamics, in contrast to the exact; as the field reduces toward the end of the pulse the ionization in either of these cases saturates, but the quasistatic fails to get the density and ionization yield correct.

The left panel of Figure 3 shows that neglecting all the electron-nuclear correlation terms except for ϵ^{app} underestimates the ionization at first, but later, as the exact ionization begins to saturate, the ionization from ϵ^{app} continues to grow, and leads ultimately to a significant overestimate of the total ionization. Even propagating on the quasistatic potential, a crude approximation given the earlier discussion, gives a better ionization yield. We see from Fig. 3 (left) that adding \mathcal{T}_n to ϵ^{app} reduces the ionization probability at all times, due to its small confining barriers as mentioned above. On the other hand, adding $\mathcal{K}^{\text{cond}}$ to ϵ^{app} increases the ion-

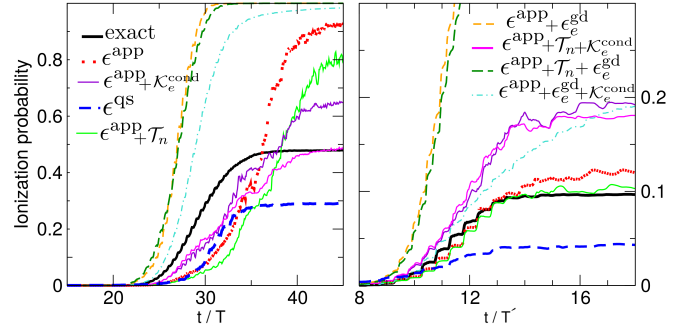


FIG. 3. Ionization yields calculated from propagating the electron on different components of the exact electronic potential as well as on the quasistatic potential. Left: $\lambda = 800$ nm and intensity $I = 2 \times 10^{14}$ W/cm² (50-cycle). Right: $\lambda = 600$ nm and intensity $I = 10^{14}$ W/cm² (20-cycle). Legends apply to both.

ization at first, and then decreases it, giving an overall somewhat improved prediction of the ionization dynamics relative to dynamics on ϵ^{app} alone. Although adding both $\mathcal{K}^{\text{cond}}$ and \mathcal{T}_n to ϵ^{app} seems to give a good final ionization yield, the intermediate dynamics is not very good. Adding ϵ_e^{gd} to ϵ^{app} drastically overshoots the ionization, yielding ultimately a completely ionized molecule. It appears for the current choice of laser parameters and initial state all these dynamical electron-nuclear correlation terms are important to include to obtain good prediction of the ionization yield. But, is this conclusion general? Does ϵ^{app} always perform so poorly?

We performed the same calculations using a 20-cycle pulse of wavelength $\lambda = 600$ nm ($\omega = 0.076$ a.u.) and intensity $I = 10^{14}$ W/cm², with a sine-squared pulse envelope. We further set the initial state to be the 6th excited vibrational state (c.f. [4]). The resulting ionization yields computed from the propagation of the electron using the different components of the exact potential is presented in the right panel of Fig. 3 ($T' = 2$ fs, is the duration of one cycle.). We see that the result of electron dynamics on ϵ^{app} in this case agrees very well with the exact result, and further, that with the addition of \mathcal{T}_n becomes even better. Other combinations of the potential components do not provide satisfactory results. In particular, once again ϵ_e^{gd} severely overestimates the ionization, while the quasistatic dynamics underestimates the ionization yield significantly. In this case, the exact potential differs substantially from the quasistatic potential from the very start, due to the vibrational excitation of the initial state.

From the discussion above it is clear that ionization dynamics depends crucially on the coupling to the quantum nuclear motion; accounting for both the splitting of the wavepacket as well as its dynamics is im-

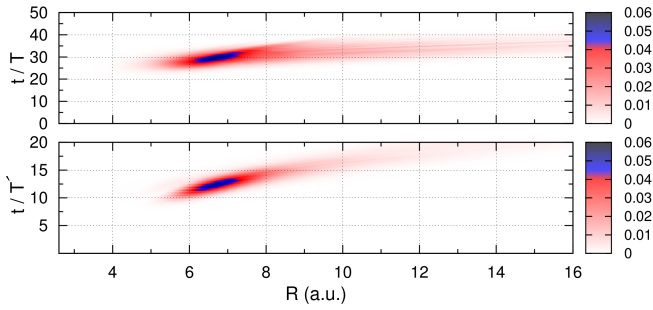


FIG. 4. Time-resolved, R -resolved, ionization probability, $I(R, t)$. Upper panel: $\lambda = 800$ nm and intensity $I = 2 \times 10^{14}$ W/cm² (50-cycle). Lower panel: $\lambda = 600$ nm and intensity $I = 10^{14}$ W/cm² (20-cycle).

portant. At this point, one may ask from which part of the nuclear wavepacket is the ionization mostly occurring? To answer this, we introduce a time-resolved, R -resolved, ionization probability via

$$I(R, t) = \int_{z_I^-} dz |\Psi(z, R, t)|^2, \quad (9)$$

with $\int_{z_I^-} = \int_{-\infty}^{-z_I} + \int_{z_I}^{\infty}$ taking $z_I = 15$ a.u., plotted in Fig 4 for *both* of the laser parameters studied in this work. In both cases, we observe a clear peak of $I(R, t)$, centered around $6 \text{ a.u.} < R < 7.5 \text{ a.u.}$, the region predicted by the quasistatic analysis of CREI, soon after the fields reach their maximum intensities. Hence, the quantity $I(R, t)$ represents a very useful measure of CREI in a fully dynamical picture, indicating clearly the dominant internuclear separations at which ionization occurs. We also point out that this quantity is analogous to the ionization probability at a given internuclear separation in the quasistatic picture [24].

In summary, we have found the exact potential driving the electron dynamics in a model one-dimensional H_2^+ molecule undergoing CREI. The presented potential provide a complete details of the CREI process beyond the quasistatic picture traditionally used to analyze and interpret this process. The large differences in the two potentials reveals the importance of dynamical electron-nuclear correlation terms lacking in previous pictures of CREI. The drastic impact these can have on the dynamics has been demonstrated, i.e. propagating the electrons in a potential that neglects these terms lead to large errors in the predictions of the ionization yield. Going beyond the quasistatic treatment by only accounting for the width and splitting of the nuclear wavepacket is generally not enough to get the correct dynamics of CREI. How significant the dynamical electron-nuclear effects are for CREI phenomena in larger systems [25] remains to be investigated, and moreover, how to accurately model them in practical approximations will

open a major avenue for future research. We further presented a time-resolved, R -resolved measure of CREI that takes into account the dynamical electron-nuclear correlation. This quantity has a clear peak in the region predicted by the quasistatic analysis of CREI, for the fields studied here, soon after the fields reach their maximum intensities.

Financial support from the National Science Foundation CHE-1152784 (N.T.M), and Department of Energy, Office of Basic Energy Sciences, Division of Chemical Sciences, Geosciences and Biosciences under Award DE-SC0008623 (E.K, A.A) are gratefully acknowledged. E.K and A.A also acknowledge financial support by the European Research Council Advanced Grant DYNAMO (ERC- 2010-AdG-267374) and Grupo Consolidado UPV/EHU del Gobierno Vasco (IT578-13).

* elham.etn@gmail.com; Corresponding author

† aliabedik@gmail.com

‡ nmaitra@hunter.cuny.edu

- [1] T. Zuo, S. Chelkowski, and A. D. Bandrauk, *Phys. Rev. A* **48**, 3837 (1993).
- [2] T. Zuo and A. D. Bandrauk, *Phys. Rev. A* **52**, R2511 (1995).
- [3] T. Seideman, M. Y. Ivanov, and P. B. Corkum, *Phys. Rev. Lett.* **75**, 2819 (1995).
- [4] S. Chelkowski, A. Conjusteau, T. Zuo, and A. D. Bandrauk, *Phys. Rev. A* **54**, 3235 (1996).
- [5] I. Ben-Itzhak, P. Q. Wang, A. M. Sayler, K. D. Carnes, M. Leonard, B. D. Esry, A. S. Alnaser, B. Ulrich, X. M. Tong, I. V. Litvinyuk, C. M. Maharjan, P. Ranitovic, T. Osipov, S. Ghimire, Z. Chang, and C. L. Cocke, *Phys. Rev. A* **78**, 063419 (2008).
- [6] E. Constant, H. Stapelfeldt, and P. B. Corkum, *Phys. Rev. Lett.* **76**, 4140 (1996).
- [7] J. Wu, M. Meckel, L. P. H. Schmidt, M. Kunitski, S. Voss, H. Sann, H. Kim, T. Jahnke, A. Czasch, and R. Dörner, *Nature communications* **3**, 1113 (2012).
- [8] S. Chelkowski, C. Foisy, and A. D. Bandrauk, *Phys. Rev. A* **57**, 1176 (1998).
- [9] S. Chelkowski and A. Bandrauk, *Journal of Physics B: Atomic, Molecular and Optical Physics* **28**, L723 (1995).
- [10] H. Yu, T. Zuo, and A. D. Bandrauk, *Journal of Physics B: Atomic, Molecular and Optical Physics* **31**, 1533 (1998).
- [11] A. D. Bandrauk and F. Légaré, in *Progress in Ultrafast Intense Laser Science VIII* (Springer, 2012) pp. 29–46.
- [12] S. Hammes-Schiffer and A. V. Soudackov, *The Journal of Physical Chemistry B* **112**, 14108 (2008).
- [13] N. Takemoto and A. Becker, *Phys. Rev. Lett.* **105**, 203004 (2010).
- [14] N. Takemoto and A. Becker, *Phys. Rev. A* **84**, 023401 (2011).
- [15] F. Légaré, I. Litvinyuk, P. Dooley, F. Quéré, A. Bandrauk, D. Villeneuve, and P. Corkum, *Phys. Rev. Lett.* **91**, 093002 (2003).
- [16] A. Abedi, N. T. Maitra, and E. K. U. Gross, *Phys. Rev. Lett.* **105**, 123002 (2010).
- [17] A. Abedi, N. T. Maitra, and E. K. U. Gross, *The Journal of Chemical Physics* **137**, 22A530 (2012).

- [18] Y. Suzuki, A. Abedi, N. T. Maitra, K. Yamashita, and E. K. U. Gross, *Phys. Rev. A* **89**, 040501 (2014).
- [19] Y. Suzuki, A. Abedi, N. T. Maitra, and E. Gross, arXiv preprint arXiv:1506.04070 (2015).
- [20] J. Javanainen, J. H. Eberly, and Q. Su, *Physical Review A* **38**, 3430 (1988).
- [21] K. C. Kulander, F. H. Mies, and K. J. Schafer, *Phys. Rev. A* **53**, 2562 (1996).
- [22] These probabilities are calculated as defined in [4]. Here we have chosen $z_I = \pm 15$ for ionization box while the dissociation box is defined as $R_D < 10$.
- [23] For the fully dynamical calculation (labelled TDSE in legend) the ionization rate at time t is calculated via $(\ln(p_v(t - T/2)) - \ln(p_v(t + T/2)))/T$ and plotted against the corresponding average internuclear separation $\langle R \rangle(t)$ at time t . Here p_v is the probability inside the ionization box. In case of CN the ionization rate is computed as given in [4].
- [24] $I(R, t)$ can be rewritten in terms of the exact conditional electronic density $|\Phi_R(z, t)|^2 = |\Psi|^2 / \int dz |\Psi|^2$ (see [16]), i.e, $I(R, t) = \int dz |\Psi|^2 \left[1 - \int_{z_I} dz |\Phi_R(z, t)|^2 \right]$. Note that $|\Phi_R|^2$ gives the conditional probability of finding electrons at z at time t , given that the internuclear separation R and can be viewed as an exactification of the electronic density for a given internuclear separation in quasistatic picture. Therefore, $I(R, t)$ can be also viewed as an exact concept analogous to the ionization probability in the quasistatic picture.
- [25] I. Bocharova, R. Karimi, E. F. Penka, J.-P. Brichta, P. Lassonde, X. Fu, J.-C. Kieffer, A. D. Bandrauk, I. Litvinyuk, J. Sanderson, *et al.*, *Phys. Rev. Lett.* **107**, 063201 (2011).